ISSN (Print) 1226-1750
ISSN (Online) 2233-6656
Journal of Magnetics 22(3), 423-429 (2017) https://doi.org/10.4283/JMAG.2017.22.3.423

Optimal Design of a Permanent Magnet Synchronous Motor to Improve Torque and Demagnetization Characteristics

Yong-Min You[1]* and Dae-Won Chung[2]

Department of [1]Automotive Engineering and [2]Electrical Engineering, Honam University, Gwangju 62399, Korea

(Received 30 May 2017, Received in final form 14 July 2017, Accepted 19 July 2017)

This study proposes an unequal air-gap model for PMSMs with the objective of reducing the torque ripple and improving the demagnetization characteristics. Shape optimization is performed to optimize the design variables of the unequal air-gap model, which are the shape of the unequal air-gap and the angle between the V-shaped permanent magnets. An optimization process was performed by the Kriging model based on Latin Hypercube Sampling (LHS), and Genetic Algorithm (GA). Finite element analysis (FEA) was also utilized to analyze the torque and demagnetization characteristics. As optimal design results, the torque ripple of the optimal model was reduced by 7.7 % and the demagnetization temperature was improved by 2.2 %.

Keywords : permanent magnet synchronous motor, unequal air-gap, torque ripple, demagnetization, finite element analysis, optimal design

1. Introduction

The study of the torque ripple of Permanent Magnet Synchronous Motors (PMSMs) has been rapidly progressing, which has resulted in the improvement in the noise and vibrations of electric vehicles. There are several ways to reduce the cogging torque such as increasing the air-gap width and pole/slot number, notches in rotor and stator teeth, and skewing of rotor and stator [1-3]. The skewing of rotor and stator has been applied to the traction motor of GM Spark and Ford Focus. Recently, new methods have been developed to improve the cogging torque, which are different widths of the permanent magnet, unequal teeth width, and skewing of the permanent magnets [4-6]. However, all the above mentioned methods have disadvantages in terms of material costs and productivity.

PMSM has been widely used in electric vehicles due to its high power density. The demand for Dysprosium-free (Dy-free) permanent magnet for PMSMs has been increasing because of a limited supply of rare earth metals. However, the demagnetization temperature is a critical factor in the use of PMSMs for electric vehicles. The demagnetization characteristics of PMSMs have become more significant because Dy-free permanent magnet has lower coercivity [7].

This study proposes an unequal air-gap model for PMSMs with the objective of reducing the torque ripple and improving the demagnetization characteristics, which are significant parameters in the application of PMSMs in electric vehicles. Shape optimization is performed to optimize the design variables of the unequal air-gap model. The optimal design variables are the shape of the unequal air-gap and the angle between the V-shaped permanent magnets. An optimization process was performed by Kriging model based on Latin Hypercube Sampling (LHS) and Genetic Algorithm (GA). Finite element analysis (FEA) was also utilized to analyze the torque and demagnetization characteristics.

2. Optimal Design of PMSM

2.1. Analysis model

Figure 1 and Table 1 show the structure and specifications of a 45 kW PMSM for an electric vehicle. The PMSM has 8 poles, 48 slots, and distributed winding. V-shaped Dy-free permanent magnets are applied to concentrate the magnetic flux. Low core loss electric steels with thickness 0.27 mm are utilized to reduce the core loss and eddy current loss. In addition, skewing of per-

*Corresponding author: Tel: +82-62-940-5499
Fax: +82-62-940-5053, e-mail: ym.you@honam.ac.kr

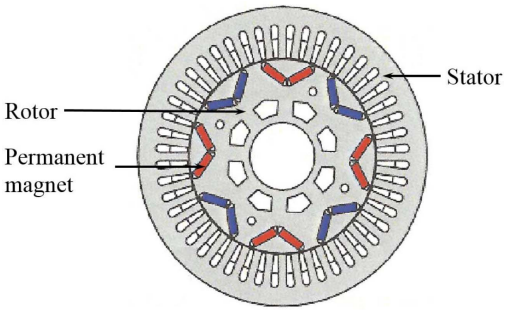

Fig. 1. (Color online) PMSM for electric vehicle.

Table 1. Specifications of analysis model.

Items		Unit	Value
Required spec.	Max. output power	kW	45
	Max. torque	N·m	120
	Rated speed	rpm	4,000
	Max. speed	rpm	12,000
Input condition	DC link voltage	Vdc	343
	Peak current	Arms	150
	Continuous current	Arms	58
Elec. and Mech. spec.	No. of poles	Poles	8
	No. of slots	EA	48
	Outer diameter	mm	185
	Lamination	mm	72
	Air gap	mm	0.7
	Winding spec.	-	ø0.85, 48 turns/phase
	Core material	-	Posco 27PNF1400
	P.M. material	-	Shinetsu N50SH-GF
	Residual flux density	G	13,800~14,400
	Coercivity	Oe	1,671~21,000

manent magnets is applied to reduce the torque ripple. Water cooling system is also applied considering high current.

Although a PMSM with non-skewing permanent magnets is considered to reduce material costs and to improve productivity, the torque ripple is 10 %, which is impossible to mass-produce. Dy-free permanent magnets are also reviewed to reduce material costs, but the demagnetization temperature is 146°C, which does not satisfy the requirement of PMSMs for electric vehicles. The required minimum demagnetization temperature of PMSM for electric vehicles is 150°C.

To apply non-skewing and Dy-free permanent magnets, an unequal air-gap is applied, as shown in Fig. 2(b), which can reduce the torque ripple and improve the demagnetization temperature. An optimal design is also performed for further improvement.

2.2. Optimal design process

Figure 3 shows an optimal design process to optimize effectively the PMSM. The objective function and constraints are established, and then decide the optimal design variables and its boundary. LHS is applied as a sampling method of the design of experiment (DOE), and FEA is utilized to analyze the fixed sampling points by

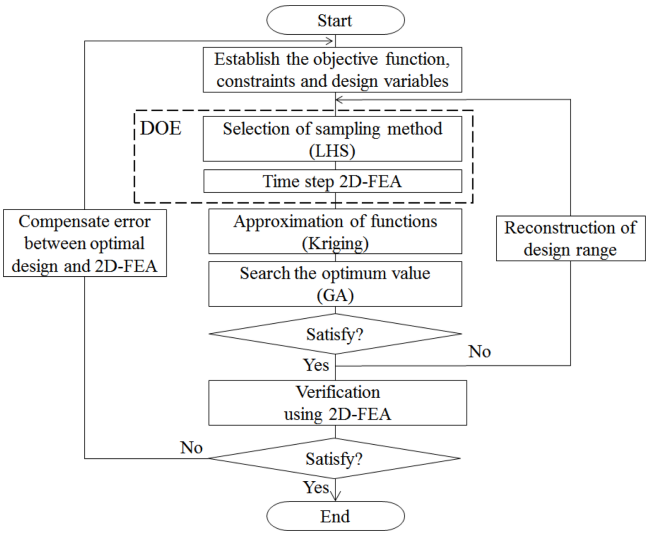

Fig. 3. Optimal design process.

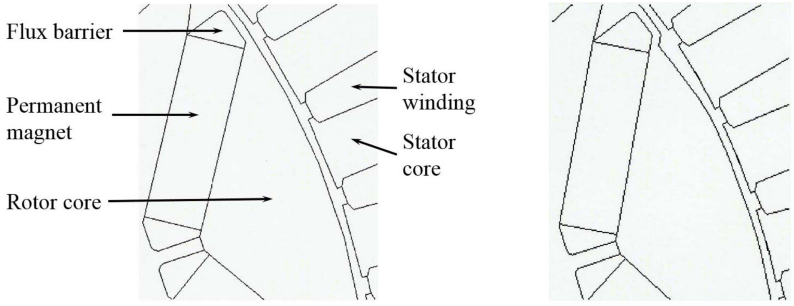

(a) Non-skew basic model (b) Unequal air-gap basic model

Fig. 2. Shape of rotor and stator.

LHS. The Kriging model is used to approximate the objective and constraints functions using DOE results. We can finally get the optimal design values by approximated Kriging model and GA, which is an optimization algorithm.

2.3. Optimal design techniques

The Kriging model is a group of geostatistical techniques used to interpolate the value of a random field. In this use of the Kriging model, the estimated equation was defined to eliminate bias and thereby minimize error variance [8]. The Kriging model is a weighted linear combination as follows.

$$z^* = \sum_{i=1}^{n} \lambda_i z_i \tag{1}$$

where z^* is an estimated point using the Kriging model, n is the total number of experiments, λ_i is the weight value function, and z_i is the experimented point.

The minimized error deviation of the Kriging model can be expressed as

$$Minimize\ \ {\sigma_{OK}}^2 = \sigma^2 - 2\sum_{i=1}^{n} \lambda_i {\sigma_{0i}}^2 + \sum_{i=1}^{n}\sum_{j=1}^{n} \lambda_i \lambda_j {\sigma_{ij}}^2 \tag{2}$$

$$With\ a\ constraint\ 1 - \sum_{i=1}^{n} \lambda_i = 0$$

where ${\sigma_{OK}}^2$ is an error variance of the Kriging model, σ^2 is a variance of z_0, ${\sigma_{0i}}^2$ is a covariance of z_0 and z_i, σ_{ij}^2 is a covariance of z_i and z_j, z_0 is a real value to predict.

When the error deviation of the Kriging model is minimized, it can be expressed as

$$L(\lambda_1, \lambda_2, \cdots, \lambda_n; \omega) = \sigma^2 - 2\sum_{i=1}^{n} \lambda_i {\sigma_{0i}}^2 + \sum_{i=1}^{n}\sum_{j=1}^{n} \lambda_i \lambda_j {\sigma_{ij}}^2 + 2\omega\left(1 - \sum_{i=1}^{n} \lambda_i\right) \tag{3}$$

where L(λ_1, λ_2,..., λ_n; ω) is a Lagrange objective function, ω is a Lagrange factor and the coefficient 2 is used for convenience.

The objective function is calculated by a partial derivative of Lagrange factor with respect to λ and ω as follows.

$$\sum_{i=1}^{n} \lambda_i {\sigma_{il}}^2 - \omega = {\sigma_{0l}}^2, l = 1, 2, \cdots, n \tag{4}$$

The error deviation of the Kriging model can be expressed as

$${\sigma_{OK}}^2 = Var(z) - \sum_{i=1}^{n} \lambda_i Cov(z_0, z_i) + \omega = \sigma^2 - \sum_{i=1}^{n} \lambda_i \sigma_{0i}^2 + \omega \tag{5}$$

LHS is a space filling design, which tends to uniformly sample points in the whole parameter space. To effectively construct the Kriging model, LHS is also used for improved accuracy over random sampling and stratified sampling to estimate the means, deviations and distribution functions of an output. Moreover, it ensures that each of the input variables represent all portions of its range.

(a) Random sampling (b) LHS

Fig. 4. (Color online) Sampling method for optimal design.

The difference between random sampling and LHS technique in the two-dimensional plane is shown in Fig. 4. A new sample point of random sampling is created without taking into account the previously generated sample points. Therefore, random sampling does not require upfront information on the necessary number of sampling points. However, the LHS technique determines the total number of sampling points before placing a sample point with matrix information.

As the final step of the optimization, GA was applied to find the optimal points of the design variables. GA is a global optimization algorithm, which is based on the evolution of the natural world. GA describes the possible solution as a specific form of the data structure. A better solution can be found by gradually transforming the possible solution. The GA will repeat the major computations, such as evaluation, creation of a mating pool, crossover operation, and mutation until the objective function meets the desired level or the maximum number of repetitions is reached.

2.4. Optimal design conditions

To improve the torque ripple and demagnetization temperature, the objective function and constraints are established as Equation (6) and (7), respectively. The objective function is to minimize the torque ripple of PMSM. The constraints are the demagnetization temperature of permanent magnets and the maximum torque of PMSM. To satisfy the objective function and the constraints, the design variables are decided as shown in Fig. 5. The design variables are the angle (X1) between the V-shaped permanent magnets and the dimensions (X2, X3) concerned with the shape of an unequal air-gap. The total number of the DOE is 15, taking into account the number of the design variables.

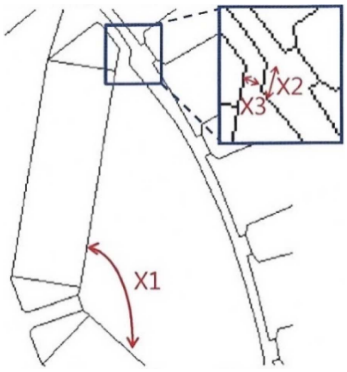

Fig. 5. (Color online) Optimal design variables.

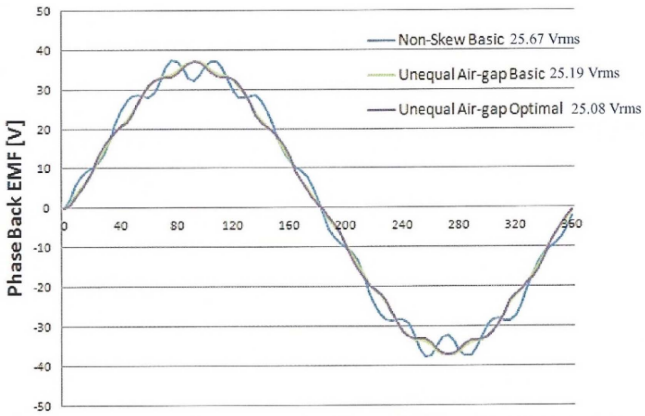

Fig. 6. (Color online) Back EMF characteristics.

• Objective function (6)
Minimize the torque ripple

• Constraints (7)
Demagnetization temperature of the permanent magnets ≥ 150 °C
Max. torque ≥ 126 N·m (5 % margin of target max. torque, which is 120 N·m)

2.5. Optimal design result

The optimal design was performed using PIANO, which is a commercial optimization program. The optimal design variables were well converged after 200 iterations. Optimal design results are shown in Table 2. The angle (X1) between the V-shaped permanent magnets was increased by 7.6° (from 116° to 123.6°), and the dimensions (X2, X3) of the unequal air-gap were also optimized.

2.5.1. Back EMF characteristics

It is easier to control a waveform that has been improved to a sinusoidal wave. The magnetic flux can flow smoothly within the magnetic circuit through the application of an unequal air-gap. As a result, the back EMF waveform was improved to a sinusoidal wave as shown in Fig. 6. The total harmonic distortion (THD) of the back EMF of the optimal model was 5.5 %, which was an improvement of approximately 2 % compared to 7.56 % of the non-skew basic model.

2.5.2. Torque characteristics

Figure 7 shows the torque characteristics when the

Table 2. Comparison of design variables.

Items		Unit	Non-skew basic model	Unequal air-gap basic model	Unequal air-gap optimal model
Design variables	X1	°	116	122	123.6
	X2	mm	-	1.04	1.09
	X3	mm	-	0.7	1.91

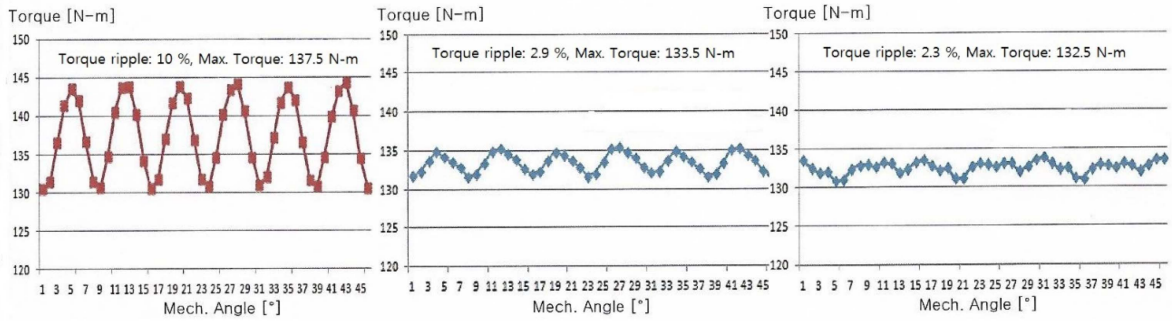

(a) Non-skew basic model (b) Unequal air-gap basic model (c) Unequal air-gap optimal model

Fig. 7. (Color online) Torque characteristics.

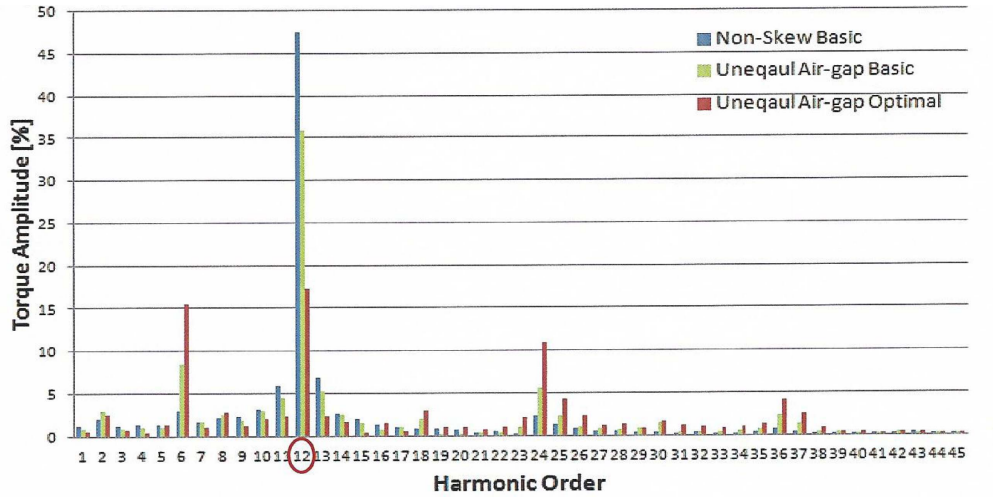

Fig. 8. (Color online) Harmonic analysis of the torque.

maximum current is applied at 900 rpm and the control angle is 47°. As shown in Fig. 7(a), the torque ripple of the non-skew basic model was approximately 10 %, which was difficult to replicate in mass production. Reduction of the torque ripple is possible by optimizing the magnetic flux distribution and reducing the magnetic saturation and space harmonics. The torque ripple was reduced to 2.9 % by applying the unequal air-gap and it was reduced to 2.3 % by the optimal design. There is a trade-off between the torque ripple and the maximum torque. Although the maximum torque was reduced slightly, it satisfied the constraint that it should be more than 126 N·m.

Figure 8 shows the harmonic analysis result of the torque. The ordinal number of harmonics influencing the torque ripple is a number that is a multiple of six. The harmonic analysis result of the three models showed that the values of the 12^{th} harmonic were the greatest. The 12^{th} harmonic of the non-skew basic model, unequal air-gap basic model, and unequal air-gap optimal model were 48 %, 36 %, and 17 %, respectively. The 12^{th} harmonic element of the optimal model was distributed over the 6^{th} and 24^{th} harmonics in the optimal design.

2.5.3. Demagnetization characteristics

The management standard for the demagnetization property of the PMSM for electric vehicles is very strict. GM manages the B-H characteristics of permanent magnets at 140°C. Hyundai Motor Co. and LG Electronics Inc. demand that permanent magnets must not be demagnetized at 150°C. A demagnetization analysis was performed under the maximum current and control angle of 150 A and 80°, respectively.

The analysis results were represented by the flux density distribution of the permanent magnets. However, the values of the flux density of permanent magnets can be converted to temperature values using the demagnetization curves of the permanent magnet. Figure 9 shows the demagnetization curves of the N50SH-GF grade of Shinetsu. The Knee points under the conditions of 140°C and 170°C are 0.4 T and 0.6 T, respectively. The simulated values of the flux density of permanent magnets can be converted to temperature values using the values of the Knee points, as established in Equation (8).

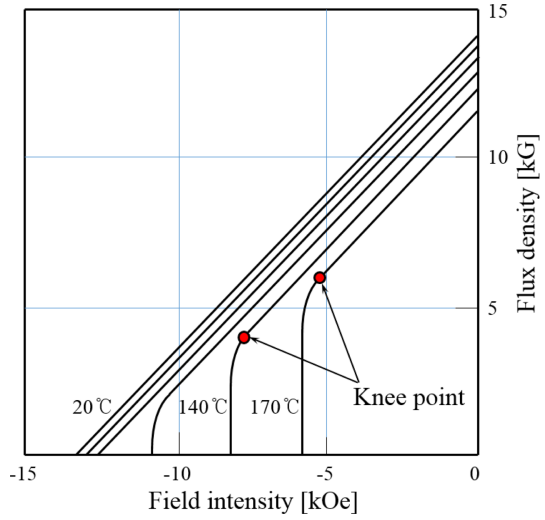

Fig. 9. (Color online) Demagnetization curves at elevated temperature (Shinetsu N50SH-GF).

$$\text{Temperature of P.M.}\,°\text{C} = 140\,°\text{C} + (170\,°\text{C} - 140\,°\text{C}) \times \frac{\text{Flux density of P.M.}\,\text{T} - 0.4\,\text{T}}{0.6\,\text{T} - 0.4\,\text{T}} \quad (8)$$

$$\text{with a constraint}: 0.4\,\text{T} \le \text{Flux density of P.M.} \le 0.6\,\text{T}$$

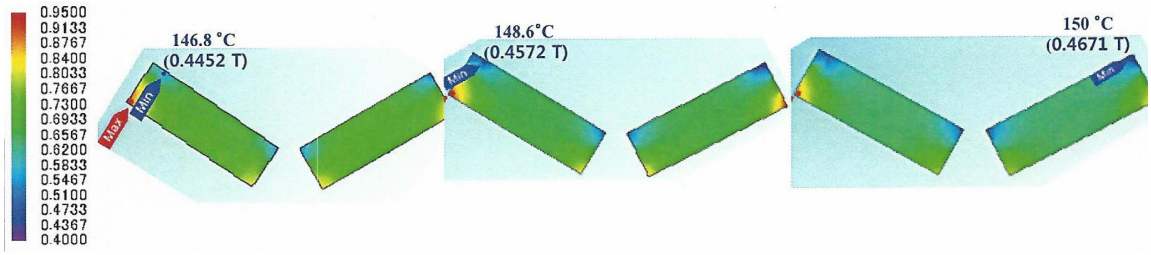

(a) Non-skew basic model (b) Unequal air-gap basic model (c) Unequal air-gap optimal model

Fig. 10. (Color online) Demagnetization characteristics.

Figure 10 shows the demagnetization analysis results of the three models. The inner edges of the permanent magnets were vulnerable to demagnetization because the magnetic flux density at these places was the lowest. The

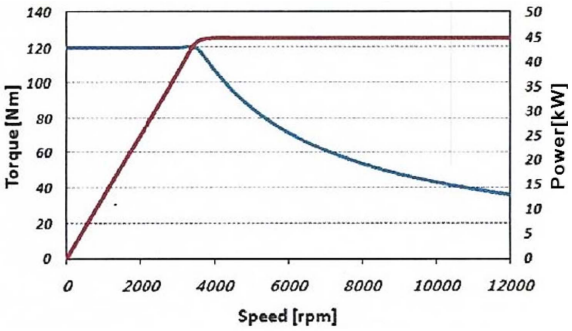

(a) Non-skew basic model

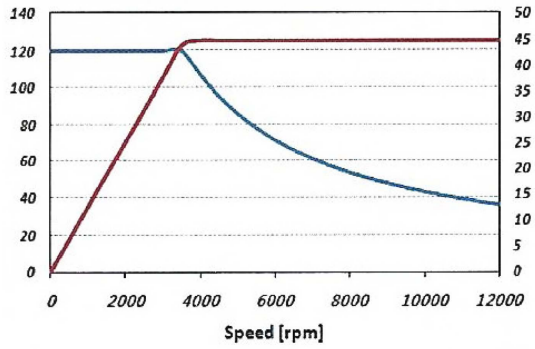

(b) Unequal air-gap basic model

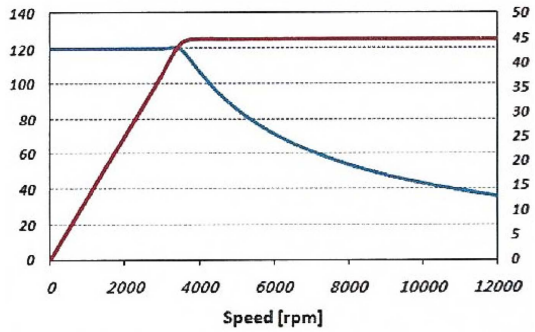

(c) Unequal air-gap optimal model

Fig. 11. (Color online) Speed-Torque characteristics.

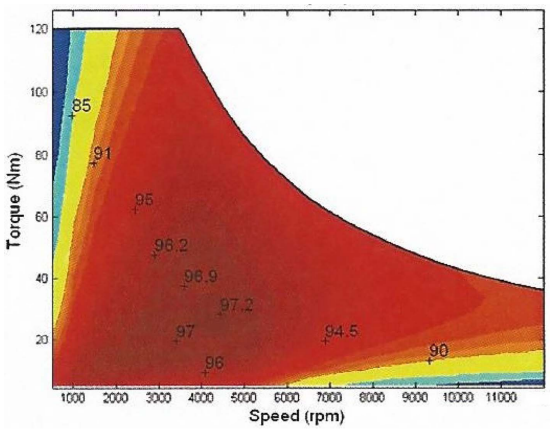

(a) Non-skew basic model

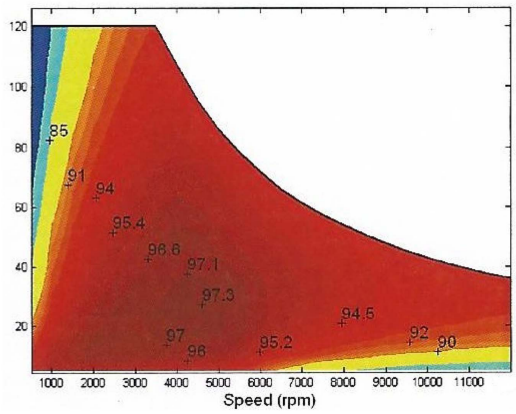

(b) Unequal air-gap basic model

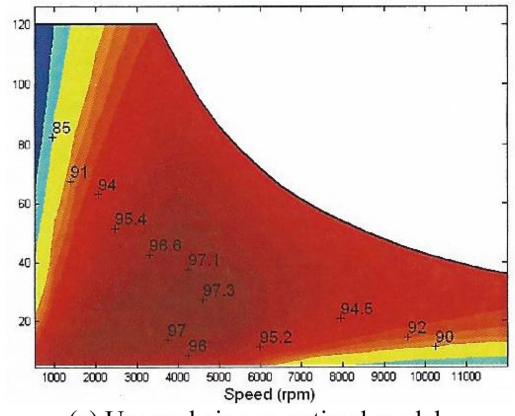

(c) Unequal air-gap optimal model

Fig. 12. (Color online) Efficiency map.

Table 3. Optimal design result

Items	Unit	Non-skew basic model	Unequal air-gap basic model	Unequal air-gap optimal model
THD of back EMF	%	7.6	5.4	5.5
Torque ripple	%	10.0	2.9	2.3
Max. torque	N·m	137.5	133.5	132.5
Demagnetization temperature	°C	146.8	148.6	150.0
Max. efficiency	%	97.2	97.3	97.3

demagnetization temperature of the non-skew basic model was 146.8°C because the minimum flux density is 0.4452 T. The demagnetization characteristic of the unequal air-gap optimal model was improved to 150°C by optimizing the angle between the V-shaped permanent magnets.

2.5.4. S-T characteristics and efficiency map

Figure 11 shows the speed-torque characteristics of the three models. The maximum torque is 120 N·m in the constant torque region until 4,000 rpm, which is the rated speed. The maximum power is 45 kW in the constant power region. The analysis results showed that the performance of the three models have similar characteristics.

The efficiency map characteristics of the three models are shown in Fig. 12. The maximum efficiency of the three models were approximately 97.2~97.3 % around the rated speed. The efficiency distributions in the entire operation region also showed no significant differences.

2.5.5. Optimal design result

Table 3 shows the optimal design result of the three models. The THD of the back EMF of the optimal model was improved 2.1 % compared to the non-skew basic model. The torque ripple of the optimal model was reduced by 7.7 % and the demagnetization temperature was improved by 2.2 % compared to the non-skew basic model. Although the maximum torque of the optimal model was reduced slightly, it satisfied the constraint of 126 N·m. The maximum efficiency of the optimal model was almost equal to the initial model.

3. Conclusion

This paper presented an unequal air-gap structure and optimal design of the PMSM for electric vehicles that can reduce the torque ripple and improved the demagnetization temperature. The angle between the V-shaped permanent magnets and the optimal dimensions of the unequal air-gap were determined using the Kriging model based on LHS and GA.

The optimization results showed that the torque ripple was reduced because the flux distribution was optimized, and the magnetic saturation and space harmonic was diminished. The demagnetization temperature was improved by optimizing the angle between the V-shaped permanent magnets. The torque ripple of the optimal model was reduced by 7.7 % and the demagnetization temperature was improved by 2.2 %.

The proposed method is expected to reduce the material costs and increase the productivity because there is no need to apply skewing of the permanent magnets. Moreover, further material cost reduction is possible by applying Dy-free permanent magnets. In conclusion, this study suggests that applying an unequal air-gap and optimized design process to the PMSM for an electric vehicle can improve the performance and contribute to cost reduction as well as productivity.

Acknowledgement

This study was supported by research fund from Honam University, 2015.

References

[1] T. W. Kim and J. H. Chang, J. Magn. **17**, 109 (2012).
[2] M. S. Islam, R. Islam, and T. Sebastian, IEEE Trans. Ind. Appl. **47**, 88 (2011).
[3] U. J. Seo, Y. D. Chun, J. H. Choi, P. W. Han, D. H. Koo, and J. Lee, IEEE Trans. Magn. **47**, 3240 (2011).
[4] M. G. Kim, G. H. Jang, C. J. Lee, and D. O. Lim, Springer **16**, 3 (2010).
[5] D. Wang and S. Y. Jung, IEEE Trans. Magn. **49**, 2295 (2013).
[6] I. Petrov, P. Ponomarev, Y. Alexandrova, and J. Pyrhonen, IEEE Trans. Magn. **51**, 8100309 (2015).
[7] B. Chen, X. Liu, R. Chen, S. Guo, C. Yan, D. Lee, and A. Yan, J. Appl. Phys. **111**, 07A710 (2012).
[8] L. Lebensztajn, C. A. R. Marretto, M. C. Costa, and J. L. Coulomb, IEEE Trans. Magn. **40**, 1196 (2004).